Scale invariant scotogenic model: CDF-II W-boson mass and the 95 GeV excesses

Amine Ahriche,[1,*] Mohamed Lamine Bellilet,[2,†] Mohammed Omer Khojali,[3,4,‡] Mukesh Kumar,[3,§] and Anza-Tshildzi Mulaudzi[3,‖]

[1]*Department of Applied Physics and Astronomy, University of Sharjah, P.O. Box 27272 Sharjah, United Arab Emirates*
[2]*Laboratoire de Physique des Rayonnements, Badji Mokhtar University, B.P. 12, 23000 Annaba, Algeria*
[3]*School of Physics and Institute for Collider Particle Physics, University of the Witwatersrand, Johannesburg, Wits 2050, South Africa*
[4]*Department of Physics, University of Khartoum, PO Box 321, Khartoum 11115, Sudan*

(Received 19 April 2024; accepted 20 June 2024; published 22 July 2024)

The anomalies observed in the W mass measurements at the CDF-II experiments and the excesses seen around 95 GeV at the Large Hadron Collider (LHC) motivate this work, in which we investigate and constrain the parameter space of the Scale Invariant Scotogenic Model with a Majorana dark matter candidate. The scanned parameters are chosen to be consistent with the dark matter relic density and the observed excesses at ∼95 GeV signal strength rates in different channels. We found that significant part of the viable space addresses the excess in the channel $\gamma\gamma$, while a tight part can address the excess in both $\gamma\gamma$ and $b\bar{b}$ channels. Furthermore, the model's viable parameters can be probed in both the LHC and future e^+e^- colliders for di-Higgs production.

DOI: 10.1103/PhysRevD.110.015025

I. INTRODUCTION

In the Standard Model (SM), the mass of the W-boson is a fundamental parameter, and precise measurements of this mass are crucial for testing the model's predictions. The reported measurements at CDF-II [1] have shown a significant discrepancy between the measured W-boson mass ($M_W^{\rm CDF} = 80.4335 \pm 0.0094$ GeV) and the mass predicted by the SM $m_W = 80.357 \pm 0.006$ GeV [2]. This discrepancy is said to be at the level of seven standard deviations. The W-boson is a weak interaction carrier; and any deviation from its SM-predicted properties, including its mass, has important implications, potentially indicating the presence of new physics beyond the Standard Model (BSM). Note that a recent measurement from ATLAS [3] ($M_W^{\rm ATLAS} = 80.370 \pm 0.019$ GeV) shows no deviation from the SM expectation. Excluding the recent measurements from CDF-II [1], the current world average from experiments yields $M_W^{\rm avg} = 80.377 \pm 0.012$ GeV, based on measurements at LEP-2 [4], Tevatron [5,6], and the LHC [7,8].

In search of a light scalar Higgs boson, the CMS and ATLAS experiments at the Large Hadron Collider (LHC) reported a local excess of 2.9σ and 1.7σ at 95.4 GeV in the di-photon ($\gamma\gamma$) invariant mass spectrum in Run 2 dataset [9–12], respectively. The Higgs-boson (H) production in the Higgsstrahlung process $e^+e^- \to ZH$ with $H \to b\bar{b}$ an excess of 2.3σ has been observed in the mass range 95 GeV $< m_H <$ 100 GeV at the LEP collider experiments [13,14]. CMS also reported another local excess in the light Higgs-boson searches in the $\tau^+\tau^-$ final state with a significance of 3.1σ which is compatible with the aforementioned excesses [15]. A recent study estimates the global significance of the excesses at 95 GeV to be 3.8σ [16].

The notable discovery of the Higgs boson at the LHC [17,18] marks the completion of the SM's foundation. Nevertheless, the observed anomalies mentioned above open new avenues for considering and constraining BSM physics. Several such studies are being considered in Refs. [16,19–39].

Despite its success, the SM has left many questions unanswered, including the hierarchy problem, the nature of dark matter (DM), and the smallness of neutrino masses. Among the extensions of the SM that address these three problems simultaneously is the Scale Invariant Scotogenic Model (SI-SCM) [40]. In this framework, the SM is

*Contact author: ahriche@sharjah.ac.ae
†Contact author: medlamine.bellilet@outlook.com
‡Contact author: khogali11@gmail.com
§Contact author: mukesh.kumar@cern.ch
‖Contact author: anza-tshilidzi.mulaudzi@cern.ch

extended by a real scalar singlet, three Majorana singlet fermions, and an inert scalar doublet. The real scalar singlet develops a vacuum expectation value (VEV) to assist in the radiatively induced electroweak symmetry breaking (EWSB), à la Coleman [41]. Here, we have two CP-even scalars whose tree-level eigenmasses are 0 and 125 GeV which correspond to a dilaton and a SM-like Higgs, respectively. When considering the radiative corrections (RCs), two scenarios are possible: (1) the dilaton mass squared acquires a positive nonzero value, $m_D < m_H$, and the Higgs mass remains $m_H = 125$ GeV (light dilaton case); and (2) the zero mass value shifts to 125 GeV due to the RCs, and the 125 GeV tree-level eigenstate becomes a heavy scalar, with $m_S > m_H$, referred as the Pure Radiative Higgs Mass (PRHM) case [42].

In this setup, the new Yukawa interactions that couple the Majorana singlet fermions and the inert scalar doublet to the lepton doublets induce a neutrino mass at one-loop level similar to the minimal scotogenic model [43]. The DM candidate here could be either a scalar (the lightest neutral inert scalar), resembling the case of the inert Higgs model extended by a real scalar [44], or the lightest Majorana singlet fermion [45]. The Majorana DM scenario in this model differs from the minimal scotogenic model, as DM annihilation occurs additionally into all SM fermions and gauge bosons via processes mediated by the Higgs boson and dilaton. This makes the new Yukawa coupling restricted only by the requirements of neutrino oscillation data and lepton flavor constraints. Here, in the setup, we investigate whether the dilaton scalar field could address the 95 GeV excess mentioned previously while considering theoretical and experimental constraints and requirements, including the DM relic density and direct detection, and the W-boson mass values measured by CDF-II. In addition, we would like to investigate the impact of all these assumptions and constraints on the di-Higgs production at the LHC (and at future e^+e^- colliders) with $\sqrt{s} = 14$ TeV (500 GeV).

This work is organized as follows: Sec. II is dedicated to presenting the SI-SCM model, describing EWSB, and discussing various theoretical and experimental constraints. Next, in Sec. III, we delve into the discussion and formulation of W mass corrections and the 95 GeV signal strength modifiers in the SI-SCM model. The di-Higgs production mechanism is detailed in Sec. IV, and our numerical results are presented and discussed in Sec. V. We conclude our work in Sec. VI.

II. MODEL AND FRAMEWORK

In the SI-SCM, the SM is extended by one inert doublet scalar, S, three singlet Majorana fermions N_i ($i = 1, 2, 3$), and one real singlet scalar ϕ to assist the radiative EWSB, as shown in Table I. The model is assigned by a global Z_2 to make the lightest Z_2-odd field stable, which plays the DM candidate role. The Lagrangian contains the following terms

TABLE I. The field charges under the symmetry Z_2, where $X_{\rm SM}$ denotes all SM fields.

Gauge group	S	N_i	ϕ	$X_{\rm SM}$
$SU(2)_L$	2	1	1	
$U(1)_Y$	−1	0	0	
Z_2	−1	−1	1	1

$$\mathcal{L} \supset -\{g_{i,\alpha}\overline{N_i^c}S^\dagger L_\beta + \text{H.c.}\} - \frac{1}{2}y_i\phi\overline{N_i^c}N_i, \tag{1}$$

where $g_{i,\alpha}$ and y_i are new Yukawa couplings; L_β are $(\ell_{\alpha R})$ the left-handed lepton doublet (right-handed leptons); the Greek letters label the SM flavors, $\alpha, \beta \in \{e, \mu, \tau\}$; and the SM Higgs and the inert scalar doublets are parametrized as: $\mathcal{H}^T = (\chi^+, (h + i\chi^0)/\sqrt{2})$ and $S^T = (S^+, (S^0 + iA^0)/\sqrt{2})$, respectively (where χ^+ and χ^0 are Goldstone bosons). The most general SI scalar potential that obeys the Z_2 symmetry is given by

$$\begin{aligned} V(\mathcal{H}, S, \phi) = {} & \frac{1}{6}\lambda_H(|\mathcal{H}|^2)^2 + \frac{\lambda_\phi}{24}\phi^4 + \frac{\lambda_S}{2}|S|^4 \\ & + \frac{\omega}{2}|\mathcal{H}|^2\phi^2 + \frac{\kappa}{2}\phi^2|S|^2 + \lambda_3|\mathcal{H}|^2|S|^2 \\ & + \lambda_4|\mathcal{H}^\dagger S|^2 + \left\{\frac{\lambda_5}{2}(\mathcal{H}^\dagger S)^2 + \text{H.c.}\right\}. \end{aligned} \tag{2}$$

The first term in Eq. (1) and the last term in Eq. (2) are responsible for generating neutrino mass via the one-loop diagrams as illustrated in Fig. 1.

The neutrino mass matrix element [46] can be written as $m_{\alpha\beta}^{(\nu)} = \sum_i g_{i,\alpha}g_{i,\beta}\Lambda_i = (g^T \cdot \Lambda \cdot g)_{\alpha\beta}$, which permits us to estimate the new Yukawa couplings using the Casas–Ibarra parametrization [47], where lepton flavor violating (LFV) bounds on the branching ratios of $\ell_\alpha \to \ell_\beta\gamma$ and $\ell_\alpha \to \ell_\beta\ell_\beta\ell_\beta$ should be fulfilled.

Here, the EWSB is triggered by the RCs where the counterterm $\delta\lambda_H, \delta\lambda_\phi, \delta\omega$, corresponding to terms in Eq. (2), are chosen to fulfill the tadpole conditions and one of the CP-even eigenmasses matches the 125 SM-like

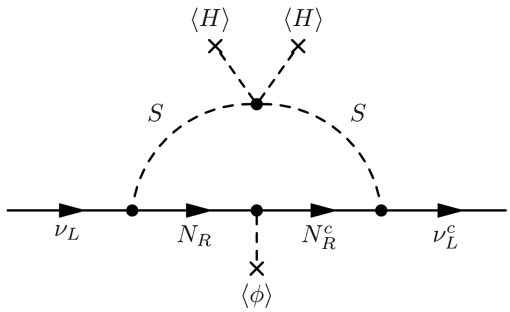

FIG. 1. The neutrino mass is generated in the SI-scotogenic model at one-loop level.

Higgs and the other corresponds to light Higgs (PRHM case) or a heavy Higgs (light dilaton case). After the EWSB ($\langle h\rangle = v, \langle\phi\rangle = x$), we obtain two CP-even eigenstates as $H = c_\alpha h - s_\alpha \phi$ and $D = s_\alpha h + c_\alpha \phi$, where H denotes the 125 GeV Higgs, D is the dilaton scalar whose mass should be around $m_D = 95.4$ GeV in this setup, and α is the Higgs-dilaton mixing angle. Here, the RCs in both PRHM and light dilaton cases ensure the mixing angle α to be in the experimental range dictated by the Higgs gauge couplings measurements. Detailed discussions on these conditions can be found in [42].

The vacuum stability must be ensured by imposing the coefficients of the term $\phi^4 \log\phi$ to be positive, which represents the leading term in the scalar; instead the term ϕ^4, where ϕ refers to any direction in the $h-\phi$ plane. Since all field dependent squared masses can be written as $m_i^2(h,\phi) = \frac{1}{2}(\alpha_i h^2 + \beta_i \phi^2)$, the vacuum stability conditions can be written as $\sum_i n_i \alpha_i^2 > 0$ and $\sum_i n_i \beta_i^2 > 0$, with n_i to be the multiplicity of the field "i." In addition to these conditions, the quartic couplings in Eq. (2) must fulfill the perturbative unitarity conditions [42].

In this model, the DM candidate could be fermionic (the lightest Majorana fermion, N_1) or a scalar (the lightest among S^0 and A^0). In the case of a scalar DM, the situation matches the singlet extended inert doublet model case [44], where the coannihilation effect should be considered in order to have viable parameters space. In the minimal scotogenic model with Majorana DM, the DM annihilation occurs via t-channel diagrams mediated by the inert fields, which makes the Yukawa couplings $g_{i,\alpha}$ values constrained by the relic density, and therefore the neutrino mass smallness can be achieved only in extreme $S^0 - A^0$ mass degeneracy, i.e., imposing a very small value for $\lambda_5 \sim \mathcal{O}(10^{-10})$ [48]. However, in the scale-invariant version, new s-channels mediated by the Higgs boson or dilaton exist, which allows all the perturbative range for the $g_{i,\alpha}$ Yukawa couplings. Also, it is worth noting that, in contrast to many Majorana dark matter models, in this model, the dark matter couples to quarks at the tree level. This feature underscores the significance of direct detection constraints on the parameter space [45].

III. M_W MEASUREMENTS & 95 GeV EXCESSES

The mass of the W-boson can be calculated as a function of the oblique parameters ΔS, ΔT, and ΔU, and is given by:

$$M_W = m_W\left[1 + \frac{\alpha}{c_W^2 - s_W^2} \times \left(-\frac{1}{2}\Delta S + c_W^2 \Delta T + \frac{c_W^2 - s_W^2}{4 s_W^2}\Delta U\right)\right]^{\frac{1}{2}}, \quad (3)$$

where $c_W = \cos\theta_W$ and $s_W = \sin\theta_W$, with θ_W being the weak mixing angle. The oblique parameters in SI-SCM model are given by [49]

$$\Delta S = \frac{1}{24\pi}\left\{(2s_W^2 - 1)^2 G(m_{S^\pm}^2, m_{S^\pm}^2, m_Z^2) + G(m_{S^0}^2, m_{A^0}^2, m_Z^2) + \log\left(\frac{m_{S^0}^2 m_{A^0}^2}{m_{S^\pm}^4}\right) + s_\alpha^2\left[\log\frac{m_D^2}{m_H^2} - \hat{G}(m_H^2, m_Z^2) + \hat{G}(m_D^2, m_Z^2)\right]\right\}, \quad (4)$$

$$\Delta T = \frac{1}{16\pi s_W^2 m_W^2}\{F(m_{S^\pm}^2, m_{S^0}^2) + F(m_{S^\pm}^2, m_{A^0}^2) - F(m_{S^0}^2, m_{A^0}^2) + 3s_\alpha^2[F(m_W^2, m_H^2) - F(m_Z^2, m_H^2) - F(m_W^2, m_D^2) + F(m_Z^2, m_D^2)]\}, \quad (5)$$

$$\Delta U = \frac{1}{24\pi}\{G(m_{S^\pm}^2, m_{S^0}^2, m_W^2) + G(m_{S^\pm}^2, m_{A^0}^2, m_W^2) - [2s_W^2 - 1]^2 G(m_{S^\pm}^2, m_{S^\pm}^2, m_Z^2) - G(m_{S^0}^2, m_{A^0}^2, m_Z^2) + s_a^2[\hat{G}(m_D^2, m_W^2) - \hat{G}(m_D^2, m_Z^2) - \hat{G}(m_H^2, m_W^2) + \hat{G}(m_H^2, m_Z^2)]\}, \quad (6)$$

where the one-loop functions G, F, and $\hat{G}$ can be found in [49].[1] The oblique parameter ΔT quantifies the contribution of new physics at low energies and ΔS at different energy scales.

In order to analyze whether the SI-SCM model can yield a shift in the prediction for M_W that is compatible with the measurements at experiments and simultaneously provides a possible explanation of the observed excesses, namely: (1) $\gamma\gamma$ & $b\bar{b}$ or (2) $\gamma\gamma$, $b\bar{b}$ & $\tau^+\tau^-$, we perform a χ^2 analysis. This analysis quantifies the agreement between the theoretically predicted signal rates $\mu_{X\bar{X}}$ [where $X = \gamma, b$ for case (1) and $X = \gamma, b, \tau$ for case (2)] and the experimentally observed values $\mu_{X\bar{X}}^{\rm exp}$. Experimentally, it was determined that the excesses at ~95 GeV were best described assuming signal rates of a scalar resonance as [10,14,15]:

$$\left.\begin{aligned}\mu_{\gamma\gamma}^{\rm exp} &= 0.27^{+0.10}_{-0.09},\\ \mu_{b\bar{b}}^{\rm exp} &= 0.117 \pm 0.057,\\ \mu_{\tau\tau}^{\rm exp} &= 1.2 \pm 0.5\end{aligned}\right\}, \quad (7)$$

where the signal strengths are defined as the cross section times the branching ratios divided by the corresponding predictions for the hypothetical SM Higgs boson at the same mass and the experimental uncertainties are given as 1σ uncertainties.

[1]Note: Subsequent to the CDF-II results, several research groups have adjusted their fits for the oblique parameters ΔS, ΔT, and ΔU in the context of electroweak precision measurements [50–52], examining their potential effects on BSM physics.

The theoretically predicted values for $\mu_{X\bar{X}}$ can be expressed as

$$\mu_{X\bar{X}} = \frac{\sigma(gg \to D) \cdot \mathcal{B}(D \to X\bar{X})}{\sigma^{\rm SM}(gg \to H) \cdot \mathcal{B}^{\rm SM}(H \to X\bar{X})} = \rho_X(1 - \mathcal{B}(D \to X_{\rm BSM})), \tag{8}$$

where ρ_X is defined for $X = \gamma,\ b,\ \tau$ as:

$$\rho_\gamma = \left| 1 + \frac{v}{2}\frac{\lambda_{DS^\pm S^\mp}}{m^2_{S^+}} \frac{A_0^{\gamma\gamma}\left(\frac{m_D^2}{4m^2_{S^+}}\right)}{A_1^{\gamma\gamma}\left(\frac{m_D^2}{4m_W^2}\right) + \frac{4}{3}A_{1/2}^{\gamma\gamma}\left(\frac{m_D^2}{4m_t^2}\right)} \right|^2,$$
$$\rho_b = \rho_\tau = s_\alpha^2, \tag{9}$$

with $X_{\rm BSM} = N_iN_k, S^0S^0, A^0A^0$. Here, $\sigma(gg \to D)$ and $\mathcal{B}(D \to X\bar{X})$ represent the ggF dilaton production and the final state $X\bar{X}$ branching ratio, respectively. The scalar triple coupling of the dilaton with charged scalars, $\lambda_{DS^\pm S^\mp}$, is given by $\lambda_{DS^\pm S^\mp} = s_\alpha\lambda_3 v + c_\alpha \kappa x$, and the loop functions $A^{\gamma\gamma}_{0,1,1/2}$ are provided in [53]. Additionally, we have $\Gamma^D_{\rm tot} = s_\alpha^2\Gamma^{D,\rm SM}_{\rm tot} + \Gamma(D \to X_{\rm BSM})$, and $\sigma^{\rm SM}(gg \to H)$ and $\mathcal{B}^{\rm SM}(H \to X\bar{X})$ are the corresponding SM quantities evaluated at the Higgs-boson mass $m_h \to m_D$ [54].

To assess the combined description of the three excesses, we define a total $\chi^2_{(N)}$ $(N = 2,\ 3)$ function as

$$\left.\begin{aligned}\chi^2_{(2)} &= \chi^2_{\gamma\gamma} + \chi^2_{b\bar{b}},\\ \chi^2_{(3)} &= \chi^2_{\gamma\gamma} + \chi^2_{b\bar{b}} + \chi^2_{\tau\tau},\end{aligned}\right\}, \tag{10}$$

and

$$\chi^2_i = \left(\frac{\mu_i - \mu_i^{\rm exp}}{\Delta\mu_i^{\rm exp}}\right)^2, \tag{11}$$

where $i = \gamma\gamma,\ b\bar{b}$, or $\tau\tau$. These functions are useful for checking whether the excess can be addressed simultaneously in the channels: (i) $\gamma\gamma, b\bar{b}$ and (ii) $\gamma\gamma, b\bar{b}, \tau\tau$.

In the parameter space region corresponding to a small charged scalar effect on the effective coupling $D\gamma\gamma$ (i.e., $\rho_\gamma \sim 1$), as indicated by the experimental values in Eq. (7), we found the following results for $\chi^2_N < 1\sigma$:

(i) $\chi^2_{(2)}|_{\rm min} = 2.262$: $s^2_\alpha = 0.11$, and $\mathcal{B}(D \to X_{\rm BSM}) = 70.15\%$.
(ii) $\chi^2_{(3)}|_{\rm min} = 7.708$: $s^2_\alpha = 0.11$, and $\mathcal{B}(D \to X_{\rm BSM}) = 69.7\%$.

This scenario becomes plausible only if the channel $D \to$ inv is accessible. Here, "inv." denotes invisible channels such as N_iN_k, H^0H^0, A^0A^0. Given that the inert neutral masses are expected to be large, the Majorana singlet fermions should be light, i.e., $m_{\rm DM} = M_1 < m_D/2$, as will be confirmed later. In the subsequent numerical analysis (Sec. V), we will consider parameter points to provide a good description of the excesses if they account for the combined effect of the excess in the channels $\gamma\gamma$ and $b\bar{b}$ at the 1σ level, since the $\tau\tau$ channel appears to be hopeless.

IV. THE DI-HIGGS PRODUCTION

In the SM, the measurement of di-Higgs (HH) production is intriguing not only because it enables the determination of Higgs-boson self-interaction but also because it contributes to understanding EWSB. In cases where EWSB proceeds via a single scalar (the SM Higgs boson), the di-Higgs signal occurs through two Feynman diagrams: box and triangle diagrams. The triangle diagram involves a triple Higgs-boson vertex that could be modified by new physics effects, represented as $\lambda_{hhh} = \lambda^{(\rm SM)}_{hhh}(1 + \Delta_{hhh})$. Therefore, the di-Higgs measurement can precisely determine the new physics effect by measuring Δ_{hhh}. However, when EWSB involves more than one scalar, as in the model considered in this study, the di-Higgs signal occurs through a box and two (or more) triangle diagrams that involve additional triple couplings λ_{hhS} (with $S = h,\ D$) and new CP scalar (dilaton in our case). Consequently, the determination of λ_{hhh} is not straightforward since $\sigma(HH)$ depends on several model parameters. Nonetheless, the experimental bounds on $\sigma(HH)$ through different channels, either via resonant or nonresonant production, are very useful for constraining the scalar sector, especially if $\sigma(HH)$ exhibits values greater than the SM predictions. Nonresonant HH production at the LHC occurs primarily through the dominant gluon fusion (ggF) mode and the subdominant vector-boson fusion (VBF) mode. The cross section for HH production at next-to-next-to-leading order, including finite top-quark-mass effects in the ggF mode, is $\sigma^{\rm SM}_{\rm ggF} = 31.05^{+2.1}_{-7.2}$ fb [55–62]. However, in the VBF mode, at next-to-next-to-next-to-leading order, the cross section is $\sigma^{\rm SM}_{\rm VBF} = 1.73 \pm 0.04$ fb [63–67] for $m_h = 125$ GeV at $\sqrt{s} = 13$ TeV. The smallness of the HH production cross section in ggF mode at leading order (LO) results from the negative interference between the box and triangle Feynman diagrams, determined by three contributing factors [42,68,69]:

$$\sigma^{\rm SM}(HH) = \sigma_B + \sigma_T + \sigma_{BT}, \tag{12}$$

where $\sigma_B = 70.1$ fb represents the box contribution, $\sigma_T = 9.66$ fb corresponds to the triangle contribution, and $\sigma_{BT} = -49.9$ fb accounts for their interference [70].

In the SI-SCM framework, nonresonant HH production through ggF mode includes an additional triangle Feynman diagram mediated through the dilaton field D. The production cross section of di-Higgs production either at the LHC or at e^-e^+ colliders has three distinct contributions that come from: (1) the Feynman diagrams involving only the triple scalar couplings that have one scalar propagator,

(2) the diagrams with only pure gauge couplings; and (3) the interference contribution [42,69]. Therefore, the di-Higgs production cross section can be expressed as follows:

$$\sigma(HH) = \zeta_1\sigma_B + \zeta_2\sigma_T + \zeta_3\sigma_{BT}, \tag{13}$$

where the coefficients ζ_i in this model are modified with respect to the SM as [69]

$$\left.\begin{aligned}\zeta_1 &= c_\alpha^4,\\ \zeta_2 &= \left|c_\alpha \tfrac{\lambda_{HHH}}{\lambda_{HHH}^{\rm SM}} + s_\alpha \tfrac{\lambda_{HHD}}{\lambda_{HHH}^{\rm SM}} \tfrac{s-m_H^2+im_H\Gamma_H}{s-m_D^2+im_D\Gamma_D}\right|^2,\\ \zeta_3 &= c_\alpha^2 \Re\left(c_\alpha \tfrac{\lambda_{HHH}}{\lambda_{HHH}^{\rm SM}} + s_\alpha \tfrac{\lambda_{HHD}}{\lambda_{HHH}^{\rm SM}} \tfrac{s-m_H^2+im_H\Gamma_H}{s-m_D^2+im_D\Gamma_D}\right)\end{aligned}\right\}, \tag{14}$$

where $\lambda_{HHH}^{\rm SM}$ is the Higgs triple coupling in the SM; and $\sqrt{s}$ is the center-of-mass collision energy, which we will consider to be $\sqrt{s} = 14$ TeV at LHC. The expression for the one-loop triple Higgs coupling in the SM is [71]:

$$\lambda_{HHH}^{\rm SM} \simeq \frac{3m_H^2}{v}\left[1 - \frac{m_t^4}{\pi^2 v^2 m_H^2}\right], \tag{15}$$

with m_t as the top quark mass.

Interestingly, a direct measurement of the triple Higgs-boson self-coupling is achievable through resonant HH production at a future e^+e^- collider. This involves double Higgsstrahlung processes with W or Z bosons, as well as through WW or ZZ fusion. In the case of double Higgsstrahlung ($e^+e^- \to HHZ$) production at $\sqrt{s} = 500$ GeV, the production cross section can be expressed as Eq. (13) using the same coefficients in Eq. (14) and the cross-section contributions given as $\sigma_B = 0.0837$ fb, $\sigma_T = 0.01565$ fb, and $\sigma_{BT} = 0.05685$ fb [42].

V. NUMERICAL RESULTS AND DISCUSSION

In this section, our attention is directed towards the parameter space corresponding to the dilaton mass window of 94 GeV $< m_D <$ 97 GeV. We systematically consider various theoretical and experimental constraints, including perturbativity, perturbative unitarity, Higgs-boson di-photon and invisible decays, LEP negative searches, and the electroweak precision tests. In addition, we require the DM relic density to match the observed values, and the DM direct detection constraints to be satisfied [45]. In our analysis, instead of relying on the bounds on the total Higgs strength modifier ($\mu_{\rm tot} = c_\alpha^2 \times (1 - \mathcal{B}_{\rm inv}) \geq 0.89$ at 95% confidence level (CL) [72]),[2] we perform a detailed analysis by considering the bounds on the Higgs total decay width ($\Gamma_h = 4.6^{+2.6}_{-2.5}$ MeV); and the partial Higgs strength signal modifiers μ_{XX}^h for $X = \mu, \tau, b, \gamma, W, Z$ [2]. For this reason, we define the SM $\chi^2_{\rm SM}$ function

$$\chi^2_{\rm SM} = \sum_{\mathcal{O}} \chi^2_{\mathcal{O}} = \sum_{\mathcal{O}} \left(\frac{\mathcal{O} - \mathcal{O}^{\rm exp}}{\Delta\mathcal{O}^{\rm exp}}\right)^2, \tag{16}$$

with the observables $\mathcal{O}$ denotes the Higgs total decay width (Γ_h) and the Higgs signal strength modifiers (μ_{XX}^h). In our analysis, we consider only benchmark points (BPs) with a precision of 95% CL, i.e., $\chi^2_{\rm SM} < 11.07$.

Additionally, we ensure that the considered values for the model's free parameters, including the inert masses ($m_{S^0}, m_{A^0}, m_{S^\pm}$), Majorana masses ($M_i$), scalar coupling λ_3, and the singlet VEV x, correspond to values of the new Yukawa couplings $g_{i,\alpha}$ that satisfy the neutrino oscillation data and LFV constraints.

Through a random numerical scan adhering to the aforementioned constraints and conditions, we consider 15,000 BPs that satisfy the 95 GeV excess in the $\gamma\gamma$ channel ($\mu_{\gamma\gamma}^{\rm exp} = 0.27^{+0.10}_{-0.09}$). The viable parameter space fulfilling the various conditions and constraints is illustrated in Fig. 2.

Figure 2(a) reveals that the assumptions of $m_D \approx$ 95 GeV and $\mu_{\gamma\gamma}^{\rm exp} = 0.27^{+0.10}_{-0.09}$ lead to inert masses exceeding 300 GeV. Additionally, the new Yukawa couplings are an order of magnitude smaller than the perturbative limit, contrasting with general cases in the SI-SCM [40,45]. From Fig. 2(a), one can observe that the couplings $g_{i,\alpha}$ have values ranging from 0.001 to 0.4 for inert masses across different ranges. These values are dictated by the requirements for DM relic density [45,48,76], where the DM annihilation channels $N_1N_1 \to \ell_\alpha\ell_\beta, \nu_\alpha\nu_\beta$ play a key role in the majority of the viable parameter space.

In Fig. 2(b), we show the singlet scalar VEV x as a function of the DM mass $m_{\rm DM}$ and the freeze-out parameter x_f. It is noteworthy that $m_{\rm DM}$ must be smaller than $m_D/2$ to ensure the branching ratio $\mathcal{B}(D \to {\rm inv})$ lies between 50% and 85%, satisfying the assumption $\mu_{\gamma\gamma}^{\rm exp} = 0.27^{+0.10}_{-0.09}$ [Fig. 2(b)]. It's important to mention that the values of the DM freeze-out observable (the annihilation cross section and freeze-out parameter $x_f = m_{\rm DM}/T_f$, where T_f is the freeze-out temperature) exhibit typical values for a Weakly Interacting Massive Particle DM candidate. One notices that the singlet scalar VEV, x, has lower bounds arising from various constraints. Perturbativity and unitarity together require $x >$ 57 GeV, which is the dominant constraint for $M_1 \equiv m_{\rm DM} \lesssim 1$ GeV. For $M_1 \equiv m_{\rm DM} > 1$ GeV, the dominant constraint comes from the Higgs-dilaton mixing, which is equivalent to $\chi^2_{\rm SM} < 11.07$. Despite the tight range of the dilaton mass, 94 GeV $< m_D <$ 97 GeV, the singlet scalar VEV spans a broad interval, $x \in [57\ {\rm GeV}, 100\ {\rm TeV}]$. This can be understood by considering that the dilaton mass is a one-loop effect sensitive to multiple parameters, including x, the

[2]Here, the Higgs invisible branching ratio is constrained by ATLAS to be $\mathcal{B}_{\rm inv} = \mathcal{B}(H \to N_iN_k) < 0.11$ [73].

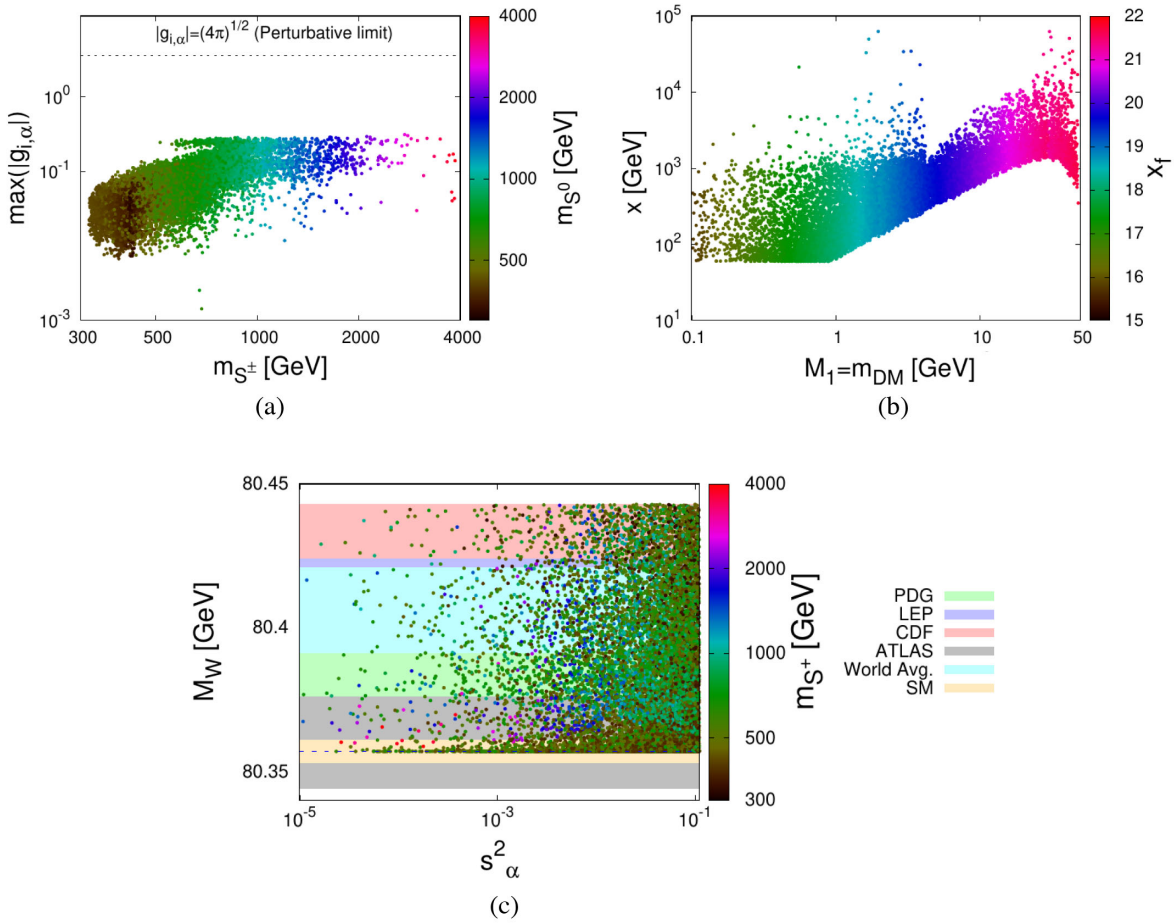

FIG. 2. (a) Maximum Yukawa couplings $\max(|g_{i,\alpha}|)$ plotted against the masses of the charged inert doublet, $m_{S^\pm}$, and the neutral scalar, m_{S^0}. (b) The singlet scalar VEV x as a function of $m_{\rm DM}$ and the freeze-out parameter, x_f. (c) M_W prediction in the SI-SCM model shown with respect to the scalar mixing angle, s^2_α, and $m_{S^\pm}$. The horizontal color bands represent M_W measurements at a 2σ level from various experiments: green for PDG [74], blue for LEP [75], red for CDF [1], gray for ATLAS [3], cyan for the world average [38], and yellow for the SM value.

multiplicity (n_i), and the couplings of the new fields to the Higgs doublet (α_i) and the singlet scalar (β_i). Thus, any value for the dilaton mass can be achieved by selecting appropriate values for the couplings (α_i, β_i), making the range of x indistinguishable for cases of restricted and nonrestricted dilaton mass [40,42,45].

In Fig. 2(c), we depict the M_W prediction within the framework of the SI-SCM model as a function of the scalar mixing angle s^2_α and $m_{S^\pm}$. Additionally, we compare these predictions with various measurements at their respective 2σ limits. Importantly, in this model, the correction Δm_W is strictly positive, driven by the fact that ΔT is always positive and dominates over the values of ΔS and ΔU. For instance, without considering the M_W bounds, the relative mass difference between CP-even and CP-odd scalars could reach 20%, whereas incorporating the M_W measurements reduces this difference to below 5%.

In Fig. 3, we present the signal strength modifiers and the relevant observable for the 95 GeV scalar candidate. Notably, the excesses $\mu_{\gamma\gamma,b\bar{b}}$ can be simultaneously addressed, whereas the excess $\mu_{\tau\tau}$ shows suppressed values. As illustrated in the $\mu_{\gamma\gamma} - \mu_{b\bar{b}}$ panels in Fig. 3, the excesses in the channels $(\gamma\gamma, b\bar{b})$ can be accommodated simultaneously at the 1σ level for a very small region of the parameter space (the BPs point inside the 1σ contour in Figs. 3(a)–3(c) with $\chi^2_{(2)} < 2.53$); and at the 2σ level for a significant region of the parameter space. However, the $\tau\tau$ channel can only be accommodated at the 99% CL, i.e., $8.02 < \chi^2_{(3)} < 11.34$. The preference for maximal values in both scalar mixing, $s^2_\alpha \approx 0.11$, and $\mathcal{B}(D \to \text{inv}) \approx 70\%$, becomes evident when matching the excess in channels other than $\gamma\gamma$ as shown in Fig. 3(d). If the di-tau excess is analyzed by ATLAS and/or reanalyzed by CMS with additional data, and the measured $\mu^{\rm exp}_{\tau\tau}$ is relaxed to around 0.6-0.7, then addressing the three excesses within this model becomes feasible.

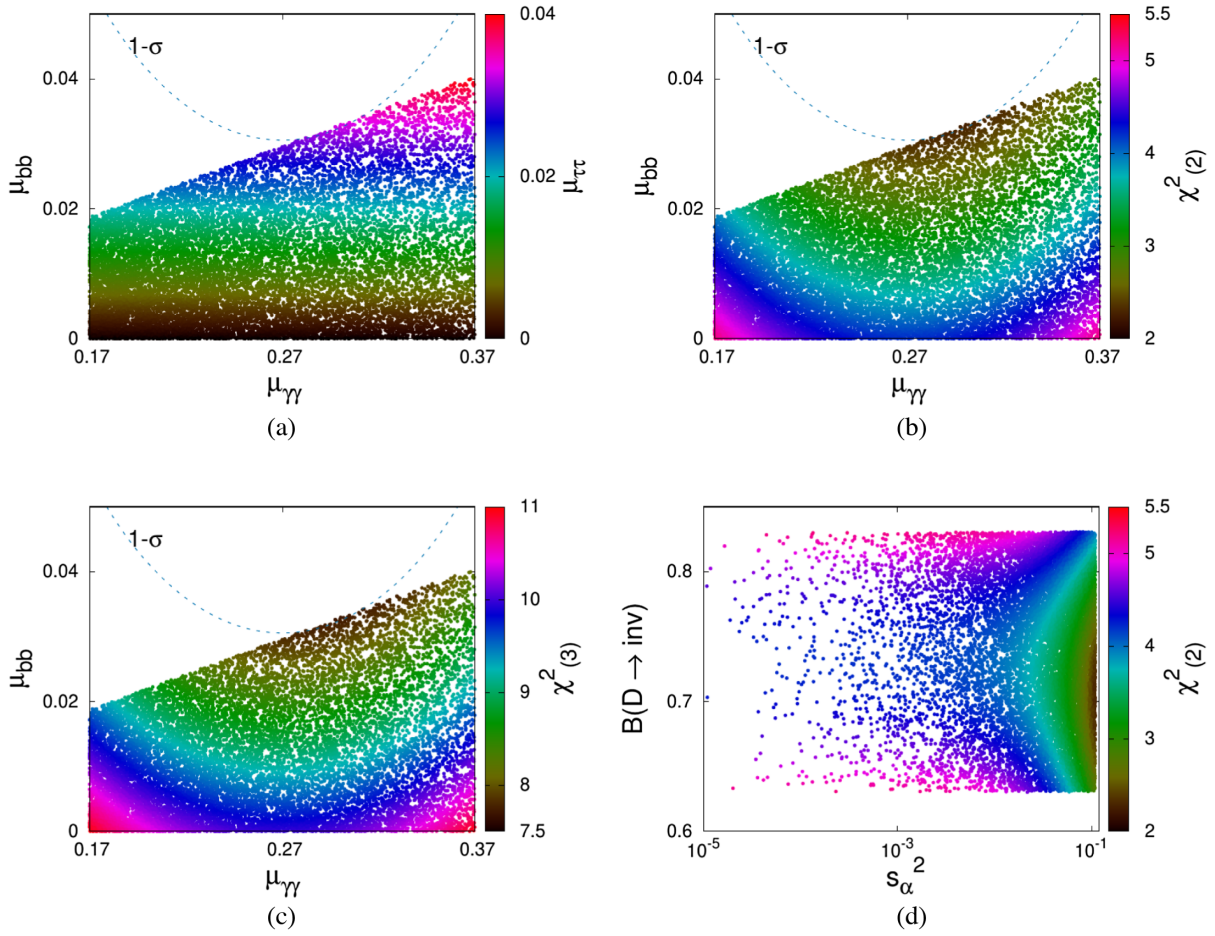

FIG. 3. (a) The plot illustrates the signal strengths for the three excesses: $\gamma\gamma$, $\tau\tau$, and $b\bar{b}$. (b) This plot presents the signal strengths of $\gamma\gamma$ and $b\bar{b}$ as functions of the total $\chi^2_{(2)}$. (c) Signal strengths of $\gamma\gamma$ and $b\bar{b}$ are plotted against the total $\chi^2_{(3)}$. (d) This plot shows the dilaton's invisible branching ratio versus the scalar mixing angle, s^2_α, presented alongside the total $\chi^2_{(2)}$. In panels (a)–(c), all the benchmark points (BPs) fall within the 2σ contour, though it is visible only in a restricted region due to the chosen $\mu_{\gamma\gamma}$ values.

In Fig. 4, we present the di-Higgs production cross section for both (a) the LHC with $\sqrt{s} = 14$ TeV and (b) future e^-e^+ colliders with $\sqrt{s} = 500$ GeV plotted against the scalar mixing angle s^2_α. As shown in Fig. 4(a), di-Higgs production at the LHC exhibits no enhancement; however, a reduction of 73% is possible for benchmark points with a smaller singlet VEV x and nonsuppressed scalar mixing. In contrast, at e^+e^- colliders, the double Higgsstrahlung cross section ranges from a reduction of 24% to an enhancement of 46% compared to the SM cross section, as illustrated in Fig. 4b.

Current constraints from the LHC [77–86], particularly those from the $HH \to \gamma\gamma b\bar{b}$ and other di-Higgs decay channels, place stringent limits on the di-Higgs production cross section and the Higgs cubic self-coupling. Our model, which predicts a nonzero branching ratio to invisible particles, must be evaluated in light of these constraints. The di-Higgs cross section predicted by our model is smaller than the SM values, inherently satisfying all the bounds from negative searches at the LHC. Given the smaller cross section, the predicted rates for $HH \to \gamma\gamma b\bar{b}$ and other di-Higgs decay channels remain below the upper limits set by the LHC. This implies that the model does not predict an excess of di-Higgs events that would have already been excluded by current experimental data.

While our results suggest that the SI-SCM model is consistent with current studies on collider anomalies, including the CDF-II W-mass anomaly and the 95 GeV excess [34,35], it is important to note that the muon's magnetic moment, $(g-2)_\mu$, anomaly cannot be addressed in this model. This limitation arises from its single negative contribution, which is insufficient to match the measured value. To reconcile this discrepancy in $(g-2)_\mu$, an extension of the SI-SCM by incorporating additional scalar components may be required. Such an extension could potentially enable the model to successfully account for the experimental values associated with $(g-2)_\mu$.

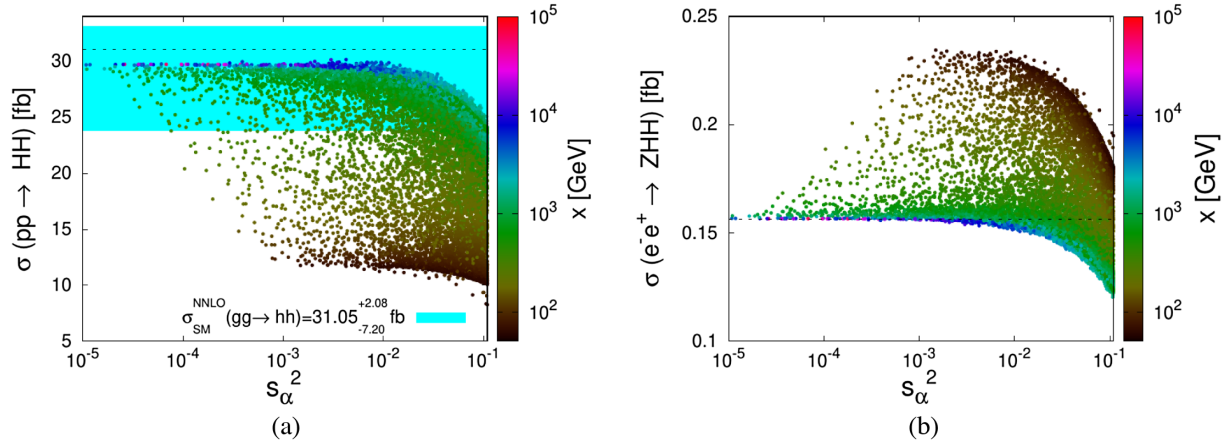

FIG. 4. The di-Higgs production cross-sections: (a) through ggF mode at the LHC with $\sqrt{s} = 14$ TeV and (b) at future e^-e^+ colliders with $\sqrt{s} = 500$ GeV, plotted against the scalar mixing angle s_α^2. The color palette represents the singlet VEV x in GeV. The black dashed lines indicate the SM predictions.

VI. CONCLUSION

In response to anomalies observed in the measurement of the W-mass at CDF-II and an excess around ∼95 GeV reported by LEP, CMS, and ATLAS, we conducted a study within the framework of the SI-SCM model to address these issues. This model, characterized by radiatively induced EWSB, not only accommodates light neutrino masses but also proposes a Majorana dark matter candidate. Its predictions are well within the reach of collider experiments. We identified a viable parameter space where inert scalar masses can explain the W-mass anomaly, and the light dilaton with $m_D \sim 95$ GeV aligns with the observations in that region. Under these assumptions, the dilaton might need to decay into invisible Majorana singlet fermions to address the excess (7) in the channels $\gamma\gamma$ & $b\bar{b}$. For this reason, the excesses considered in this study can be accommodated simultaneously at the 1σ level within a very small region of the parameter space, and at the 2σ level within a significant region. Within this parameter space, di-Higgs production at the LHC shows no enhancement compared to the SM. However, at e^+e^- colliders, the double Higgsstrahlung cross section varies from a reduction of 24% to an enhancement of 46% compared to the SM cross section.

ACKNOWLEDGMENTS

A. A. and M. L. B. were funded by the University of Sharjah under the research Projects No. 21021430107 "*Hunting for New Physics at Colliders*" and No. 23021430135 "*Terascale Physics: Colliders vs Cosmology*."

[1] T. Aaltonen *et al.* (CDF Collaboration), Science **376**, 170 (2022).
[2] R. L. Workman *et al.* (Particle Data Group), Prog. Theor. Exp. Phys. **2022**, 083C01 (2022).
[3] ATLAS Collaboration, Report No. ATLAS-CONF-2023-004.
[4] S. Schael *et al.* (ALEPH, DELPHI, L3, OPAL, and LEP Electroweak Collaborations), Phys. Rep. **532**, 119 (2013).
[5] T. Aaltonen *et al.* (CDF Collaboration), Phys. Rev. Lett. **108**, 151803 (2012).
[6] V. M. Abazov *et al.* (D0 Collaboration), Phys. Rev. D **89**, 012005 (2014).
[7] M. Aaboud *et al.* (ATLAS Collaboration), Eur. Phys. J. C **78**, 110 (2018); **78**, 898(E) (2018).
[8] R. Aaij *et al.* (LHCb Collaboration), J. High Energy Phys. 01 (2022) 036.
[9] A. M. Sirunyan *et al.* (CMS Collaboration), Phys. Lett. B **793**, 320 (2019).
[10] T. Biekoetter, S. Heinemeyer, and G. Weiglein, Phys. Rev. D **109**, 035005 (2024).
[11] CMS Collaboration, Report No. CMS-PAS-HIG-20-002.
[12] ATLAS Collaboration, Report No. ATLAS-CONF-2023-035.
[13] R. Barate *et al.* (LEP Working Group for Higgs Boson Searches, ALEPH, DELPHI, L3, and OPAL Collaborations), Phys. Lett. B **565**, 61 (2003).
[14] G. Abbiendi *et al.* (OPAL Collaboration), Eur. Phys. J. C **27**, 311 (2003).

[15] A. Tumasyan *et al.* (CMS Collaboration), J. High Energy Phys. 07 (2023) 073.
[16] S. Bhattacharya, G. Coloretti, A. Crivellin, S. E. Dahbi, Y. Fang, M. Kumar, and B. Mellado, arXiv:2306.17209.
[17] G. Aad *et al.* (ATLAS Collaboration), Phys. Lett. B **716**, 1 (2012).
[18] S. Chatrchyan *et al.* (CMS Collaboration), Phys. Lett. B **716**, 30 (2012).
[19] G. Cacciapaglia, A. Deandrea, S. Gascon-Shotkin, S. Le Corre, M. Lethuillier, and J. Tao, J. High Energy Phys. 12 (2016) 068.
[20] A. Crivellin, J. Heeck, and D. Moeller, Phys. Rev. D **97**, 035008 (2018).
[21] J. Cao, X. Jia, Y. Yue, H. Zhou, and P. Zhu, Phys. Rev. D **101**, 055008 (2020).
[22] T. Biekoetter, M. Chakraborti, and S. Heinemeyer, Eur. Phys. J. C **80**, 2 (2020).
[23] J. M. Cline and T. Toma, Phys. Rev. D **100**, 035023 (2019).
[24] A. A. Abdelalim, B. Das, S. Khalil, and S. Moretti, Nucl. Phys. **B985**, 116013 (2022).
[25] S. Heinemeyer, C. Li, F. Lika, G. Moortgat-Pick, and S. Paasch, Phys. Rev. D **106**, 075003 (2022).
[26] T. Biekoetter, A. Grohsjean, S. Heinemeyer, C. Schwanenberger, and G. Weiglein, Eur. Phys. J. C **82**, 178 (2022).
[27] T. Biekoetter and M. O. Olea-Romacho, J. High Energy Phys. 10 (2021) 215.
[28] W. Li, J. Zhu, K. Wang, S. Ma, P. Tian, and H. Qiao, Chin. Phys. C **47**, 123102 (2023).
[29] S. Iguro, T. Kitahara, and Y. Omura, Eur. Phys. J. C **82**, 1053 (2022).
[30] T. Biekoetter, S. Heinemeyer, and G. Weiglein, J. High Energy Phys. 08 (2022) 201.
[31] R. Benbrik, M. Boukidi, S. Moretti, and S. Semlali, Phys. Lett. B **832**, 137245 (2022).
[32] T. Biekoetter, S. Heinemeyer, and G. Weiglein, Eur. Phys. J. C **83**, 450 (2023).
[33] F. J. Botella, F. Cornet-Gomez, C. Mire, and M. Nebot, Eur. Phys. J. C **82**, 915 (2022).
[34] P. Escribano, V. M. Lozano, and A. Vicente, Phys. Rev. D **108**, 115001 (2023).
[35] D. Borah, S. Mahapatra, P. K. Paul, and N. Sahu, Phys. Rev. D **109**, 055021 (2024).
[36] G. Coloretti, A. Crivellin, S. Bhattacharya, and B. Mellado, Phys. Rev. D **108**, 035026 (2023).
[37] H. Abouabid, A. Arhrib, R. Benbrik, M. Boukidi, and J. E. Falaki, J. Phys. G **51**, 075001 (2024).
[38] S. Ashanujjaman, S. Banik, G. Coloretti, A. Crivellin, B. Mellado, and A. T. Mulaudzi, Phys. Rev. D **108**, L091704 (2023).
[39] A. Ahriche, arXiv:2312.10484.
[40] A. Ahriche, K. L. McDonald, and S. Nasri, J. High Energy Phys. 06 (2016) 182.
[41] S. R. Coleman and E. J. Weinberg, Phys. Rev. D **7**, 1888 (1973).
[42] A. Ahriche, Nucl. Phys. **B982**, 115896 (2022).
[43] E. Ma, Phys. Rev. D **73**, 077301 (2006).
[44] M. O. Khojali, A. Abdalgabar, A. Ahriche, and A. S. Cornell, Phys. Rev. D **106**, 095039 (2022).
[45] R. Soualah and A. Ahriche, Phys. Rev. D **105**, 055017 (2022).
[46] A. Merle and M. Platscher, Phys. Rev. D **92**, 095002 (2015).
[47] J. A. Casas and A. Ibarra, Nucl. Phys. **B618**, 171 (2001).
[48] A. Ahriche, A. Jueid, and S. Nasri, Phys. Lett. B **814**, 136077 (2021).
[49] W. Grimus, L. Lavoura, O. M. Ogreid, and P. Osland, Nucl. Phys. **B801**, 81 (2008).
[50] S. Centelles Chuli, R. Srivastava, and S. Yadav, Mod. Phys. Lett. A **38**, 2350049 (2023).
[51] H. Flacher, M. Goebel, J. Haller, A. Hocker, K. Monig, and J. Stelzer, Eur. Phys. J. C **60**, 543 (2009); **71**, 1718(E) (2011).
[52] P. Asadi, C. Cesarotti, K. Fraser, S. Homiller, and A. Parikh, Phys. Rev. D **108**, 055026 (2023).
[53] A. Djouadi, Phys. Rep. **457**, 1 (2008).
[54] The LHC Higgs Working Group, https://twiki.cern.ch/twiki/bin/view/LHCPhysics/LHCHWG.
[55] S. Dawson, S. Dittmaier, and M. Spira, Phys. Rev. D **58**, 115012 (1998).
[56] S. Borowka, N. Greiner, G. Heinrich, S. P. Jones, M. Kerner, J. Schlenk, U. Schubert, and T. Zirke, Phys. Rev. Lett. **117**, 012001 (2016); **117**, 079901(E) (2016).
[57] J. Baglio, F. Campanario, S. Glaus, M. Muhlleitner, M. Spira, and J. Streicher, Eur. Phys. J. C **79**, 459 (2019).
[58] D. de Florian and J. Mazzitelli, Phys. Rev. Lett. **111**, 201801 (2013).
[59] D. Y. Shao, C. S. Li, H. T. Li, and J. Wang, J. High Energy Phys. 07 (2013) 169.
[60] D. de Florian and J. Mazzitelli, J. High Energy Phys. 09 (2015) 053.
[61] M. Grazzini, G. Heinrich, S. Jones, S. Kallweit, M. Kerner, J. M. Lindert, and J. Mazzitelli, J. High Energy Phys. 05 (2018) 059.
[62] J. Baglio, F. Campanario, S. Glaus, M. Muhlleitner, J. Ronca, and M. Spira, Phys. Rev. D **103**, 056002 (2021).
[63] J. Baglio, A. Djouadi, R. Groeber, M. M. Muhlleitner, J. Quevillon, and M. Spira, J. High Energy Phys. 04 (2013) 151.
[64] R. Frederix, S. Frixione, V. Hirschi, F. Maltoni, O. Mattelaer, P. Torrielli, E. Vryonidou, and M. Zaro, Phys. Lett. B **732**, 142 (2014).
[65] L. S. Ling, R. Y. Zhang, W. G. Ma, L. Guo, W. H. Li, and X. Z. Li, Phys. Rev. D **89**, 073001 (2014).
[66] F. A. Dreyer and A. Karlberg, Phys. Rev. D **99**, 074028 (2019).
[67] F. A. Dreyer and A. Karlberg, Phys. Rev. D **98**, 114016 (2018).
[68] N. Baouche, A. Ahriche, G. Faisel, and S. Nasri, Phys. Rev. D **104**, 075022 (2021).
[69] A. Ahriche, A. Arhrib, and S. Nasri, Phys. Lett. B **743**, 279 (2015).
[70] M. Spira, arXiv:hep-ph/9510347.
[71] S. Kanemura, Y. Okada, E. Senaha, and C. P. Yuan, Phys. Rev. D **70**, 115002 (2004).
[72] G. Aad *et al.* (ATLAS and CMS Collaborations), J. High Energy Phys. 08 (2016) 045.
[73] ATLAS Collaboration, Report No. ATLAS-CONF-2020-052.

[74] C. T. Lu, L. Wu, Y. Wu, and B. Zhu, Phys. Rev. D **106**, 035034 (2022).
[75] L3 Collaboration, Eur. Phys. J. C **45**, 569 (2006).
[76] A. Ahriche, A. Jueid, and S. Nasri, Phys. Rev. D **97**, 095012 (2018).
[77] G. Aad *et al.* (ATLAS Collaboration), Phys. Rev. D **106**, 052001 (2022).
[78] G. Aad *et al.* (ATLAS Collaboration), J. High Energy Phys. 01 (2024) 066.
[79] G. Aad *et al.* (ATLAS Collaboration), Phys. Rev. D **105**, 092002 (2022).
[80] G. Aad *et al.* (ATLAS Collaboration), J. High Energy Phys. 07 (2023) 040.
[81] G. Aad *et al.* (ATLAS Collaboration), Eur. Phys. J. C **83**, 519 (2023).
[82] G. Aad *et al.* (ATLAS Collaboration), Phys. Rev. D **108**, 052003 (2023).
[83] G. Aad *et al.* (ATLAS Collaboration), J. High Energy Phys. 02 (2024) 037.
[84] G. Aad *et al.* (ATLAS Collaboration), arXiv:2404.12660.
[85] G. Aad *et al.* (ATLAS Collaboration), arXiv:2404.17193.
[86] G. Aad *et al.* (ATLAS Collaboration), arXiv:2405.20040.